Journal of Analysis and Testing (2022) 6:163–177
https://doi.org/10.1007/s41664-022-00224-0

REVIEW

Metal–Organic Frameworks-Mediated Assembly of Gold Nanoclusters for Sensing Applications

Zi-Jian Wang[1] · Qiang Li[2] · Li-Li Tan[2] · Chun-Guo Liu[1] · Li Shang[2]

Received: 14 February 2022 / Accepted: 25 March 2022 / Published online: 7 May 2022

Abstract

Gold nanoclusters (AuNCs) are an emerging type of ultrasmall nanomaterials possessing unique physicochemical characteristics. Metal–organic frameworks (MOFs), a singular kind of porous solid and crystalline material, have attracted tremendous attention in recent years. The combination of AuNCs and MOFs can integrate and improve the prominent properties of both components, such as high catalytic activities, tunable optical properties, good biocompatibility, surface functionality and stability, which make the composites of MOFs and AuNCs promising for sensing applications. This review systematically summarizes the recent progress on the sensing of various analytes via MOFs-mediated AuNCs assemblies based on strategies of luminescence sensing, colorimetric sensing, electrochemiluminescence sensing, and electrochemical and photoelectrochemical sensing. A brief outlook regarding the future development of MOFs-mediated AuNCs assemblies for sensing application is presented as well.

Keywords Gold nanoclusters · Metal–organic frameworks · Luminescence · Sensing

1 Introduction

Over the past few decades, nanomaterials have aroused extensive interests owing to their various distinct physicochemical properties [1–5]. Gold nanoclusters (AuNCs), consisting of a certain amount of gold atoms from several to a hundred, are a kind of novel nanomaterials emerging in recent years [6–11]. Benefiting from the remarkable physicochemical characteristics and fascinating architecture, plenty of attention has been paid to AuNCs in the past decades [12–17]. AuNCs possess ultrasmall core size (usually less than 2 nm), which bridges the gap between plasmonic gold nanoparticles and gold atoms. Inimitably, because the ultrasmall core size of AuNCs is approximate to the Fermi wavelength of gold [7, 18], they possess discrete energy levels and exhibit many molecule-like characteristics, for instance, discrete redox state [19], magnetism [20], molecular chirality [21], HOMO–LUMO transition [22], and photoluminescence behavior [9, 23]. In addition, AuNCs also possess merits of prominent photostability [24], high fraction of surface atoms [25] and large Stokes shift [26]. Significantly, characteristics of AuNCs, such as emission colors, surface ligands, chemical compositions and core sizes, can also be regulated facilely via various synthesis strategies. On account of the advantages mentioned above, AuNCs have been widely applied in various fields, including catalysis [25, 27], bioimaging [28, 29], sensing [30, 31], anticancer therapy [32], and antisepsis [33–35]. Particularly, in sensing fields, AuNCs have been intensively exploited as novel probes for the sensing of a wide range of different analytes, such as metal ions [36, 37], biomolecules [38, 39], temperature [40], small molecules [41], bacteria [42], cancer cells [43], and so on.

Metal–organic frameworks (MOFs) are a kind of porous materials constructed by the coordination of metal ions with organic linkers. On account of the periodic porosity

✉ Li-Li Tan
tanlili@nwpu.edu.cn

✉ Chun-Guo Liu
liucg@jlu.edu.cn

✉ Li Shang
li.shang@nwpu.edu.cn

[1] Roll-Forging Research Institute, College of Materials Science and Engineering, Jilin University, Changchun 130025, China

[2] State Key Laboratory of Solidification Processing, School of Materials Science and Engineering, Chongqing Science and Technology Innovation Center, Northwestern Polytechnical University, Xi'an 710072, China

and tunable structural characteristic, versatile functionality, chemical/thermal stability, and high surface area, MOFs hold great potential as multifunctional platforms for theranostics [44–46], catalysis [47, 48], gas storage and separation [49, 50], energy storage and conversion [51, 52], optoelectronics [53, 54], etc. Significantly, due to the distinct characteristics of tunable luminescence [55], optical absorbance [56], conductivity [57], and catalytic activity [58, 59], MOFs have also been widely exploited for the development of various sensors in recent years [60–64].

The remarkable performance of MOFs inspired their integration with AuNCs, which endowed the MOFs-mediated AuNCs assemblies (MOF/AuNCs assemblies) with enhanced selectivity, sensitivity, regenerability, and recyclability for sensing. MOF/AuNCs assemblies, possessing distinct advantages compared to other reported AuNCs-based nanocomposites due to the unique performance of MOFs [12, 77], have been proved to be a powerful analytical platform for luminescence sensing [65–69], colorimetric sensing [70, 71], electrochemiluminescence sensing [72, 73], and (photo)electrochemical sensing [74–76] (Fig. 1). Diverse types of MOFs have been introduced for the fabrication of MOF/AuNCs assemblies, including materials of institute Lavoisier MOFs (MILs) [65], zeolitic imidazolate frameworks (ZIFs) [70], cyclodextrin-based MOFs (CD-MOFs) [71], and zirconium-coordinated MOFs (Zr-MOFs) [67].

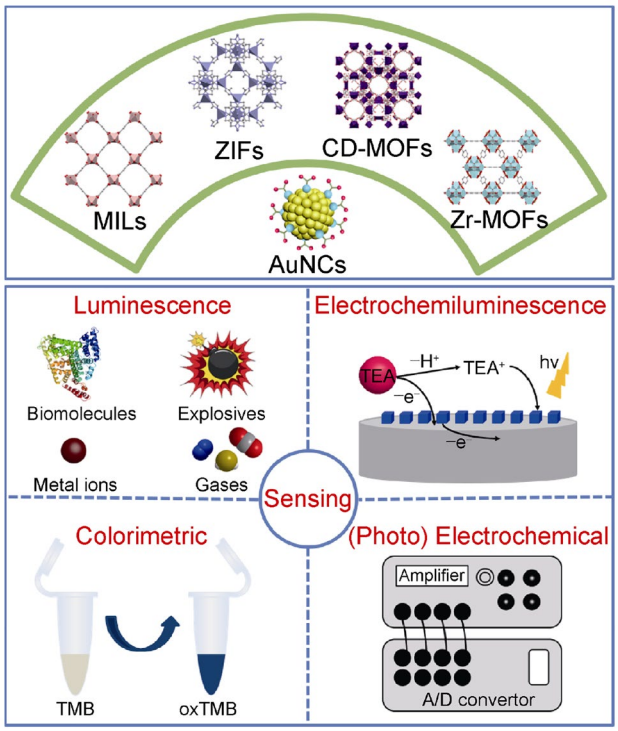

Fig. 1 Schematic illustration of sensing based on MOFs-mediated AuNCs assemblies via diverse strategies

The main advantageous features of MOF/AuNCs assemblies for sensing applications are as follows:

1) Due to the protection of MOFs, the formation of MOF/AuNCs assemblies can significantly enhance the stability of AuNCs against the environmental perturbation.
2) The photoluminescence and electrochemiluminescence performance can be remarkably improved upon MOFs' capability to inhibit the nonradiative transition of AuNCs due to the rotation and vibration of surface ligands.
3) The presence of metal anodes and abundant pores facilitates the electron transfer and reactant transport process in the catalysis reaction, which favors the colorimetric sensing based on enzyme-like catalysis of MOF/AuNCs assemblies.
4) The large surface areas and porosity of MOFs endow MOF/AuNCs assemblies with the ability to accommodate and preconcentrate analytes via host–guest interactions, which is advantageous for the ultrasensitive detection.
5) Benefiting from the size-exclusion effects and selective host–guest interactions of pores in MOF/AuNCs assemblies, the selectivity can be efficiently improved.

2 Luminescence Sensing

The tunable photoluminescence is one of the most attractive characteristic of AuNCs, which is beneficial to the development of sensitive luminescence sensing. MOF/AuNCs assemblies exhibit various advantages for enhanced sensitive and selective luminescence sensing on account of the improved properties [70]. For instance, the fluorescence intensity and lifetime of AuNCs are greatly increased in the assemblies, mainly because their nonradiative transition is attenuated due to the restriction of MOF structures [78]. In addition, the combination can also endow the assemblies with enhanced stability, intelligent responsiveness, versatile functions, etc. In this section, we will introduce important progresses made by employing MOF/AuNCs assemblies in luminescence sensing of different types of analytes.

2.1 Biomolecules

To realize minimum adverse events and optimum therapeutic efficacy, the monitoring of therapeutic drug plays an important role [78–82]. Nevertheless, the majority of drugs exhibit diverse performances involving the pharmacodynamics and pharmacokinetics; thus, it is urgent to evaluate the therapeutic response. Consequently, MOF/AuNCs assemblies have been developed for the research of personalized therapy by monitoring the delivery of drugs [78–82]. For

instance, NH_2-MIL-101(Fe) MOFs were selected as a nanocarrier to encapsulate the anticancer drug of camptothecin (Cam) (Fig. 2) [65]. Then the Cam@MOF was modified by pegylated folate (FA) to specifically recognize FA receptor locating on the membrane of cancer cells, which greatly enhanced the delivery efficiency. Meanwhile, peptide-protected AuNCs were connected onto the surface of Cam@MOF, harvesting AuNC/Cam@MOF nanoprobe with the fluorescence of AuNCs being quenched. The intercellular delivery of Cam induced programmed apoptosis and promoted the generation of caspase-3, as the apoptosis indicators, resulting in the cleavage of peptide linker between MOFs and AuNCs. As a result, the quenched fluorescence of AuNCs was turned on. By imaging the fluorescence in HepG2 cells, the targeted drug delivery could be monitored in real time. In addition, via inductively coupled plasma mass spectrometry (ICP-MS), the quantification of caspase-3 could be realized with the aid of detection of Au in the released AuNCs. The detection limit of Au was 0.12 ng/mL. Moreover, this multifunctional nanoprobe could be also

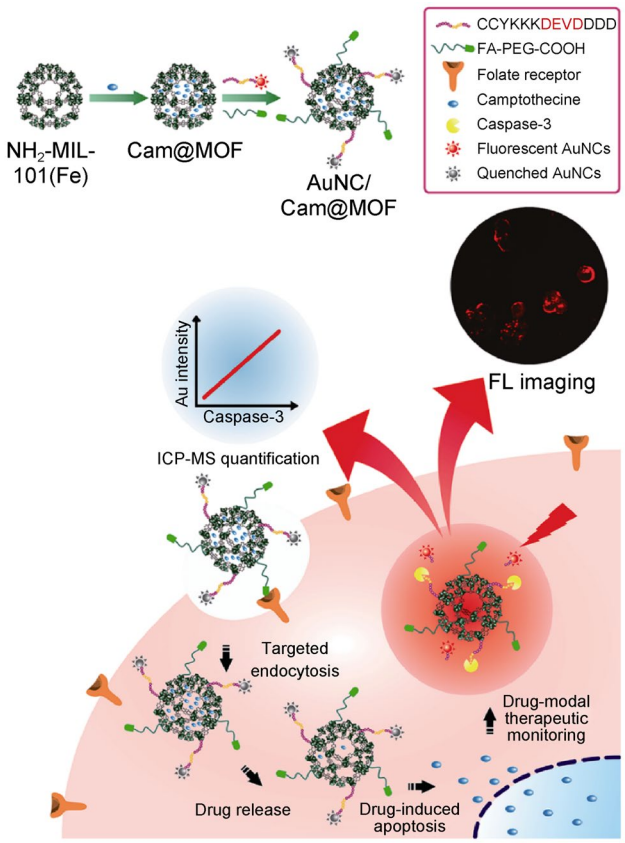

Fig. 2 Schematic depiction of fabricating multifunctional AuNC/Cam@MOF nanoprobe and the detection process. Reproduced with permission from Ref [65]. Copyright 2019, American Chemical Society

applied to the quantitative analysis and simultaneous evaluation of multiple intracellular markers.

Cysteine (Cys) is a type of sulfur-containing amino acid, which is extremely significant in regard to human body due to its versatile biological functions [83]. The content of Cys plays a role of a medical biomarker closely related to a number of diseases such as cancers, skin lesions, liver damage, edema and hair depigmentation. Consequently, it is intriguing to exploit a simple, rapid and sensitive Cys sensor for the early diagnosis of a variety of diseases. Fluorimetric test strips based on ZIFs (ZIF-8, a kind of zinc-coordinated MOFs) and Au–Ag NCs were recently exploited to monitor trace Cys in HeLa cells [66]. Nanospheres composed of Au–Ag NCs were obtained with the desolvation method, which exhibited strong fluorescence and could be selectively quenched by Cys. Through vacuum-aided fast drying strategy with super-hydrophobic patterns, these nanospheres were firstly coated onto test strips and then further covered by ZIF-8. The resulting fluorimetric test strips possess improved fluorescence, storage and environmental stabilities due to the ZIF-8 coating. Besides the detection of Cys levels in serum samples, the fabricated fluorimetric test strips can also facilely and directly detect the concentrations of Cys in HeLa cells with a linear range from 0.0032 to 32.0 μmol/L. Thus, this fluorimetric test strip based on ZIF-8 and Au–Ag NCs holds the potential to monitor trace Cys in real time for the early diagnosis of cancers clinically. Similarly, bilirubin and 3-nitrotyrosine could also be detected by AuNCs@ZIF-8 with the detection limit of 0.07 μmol/L and 1.8 nmol/L, respectively [84, 85].

Reactive oxygen species (ROS) are a kind of significant signaling molecules valuable for redox balance of life events, and the excessive accumulation of ROS will induce diverse pathological and physiological processes [86]. The highly reactive oxygen species (hROS), such as peroxynitrite ($ONOO^-$), hydroxyl radical (·OH) and hypochlorite (ClO^-), possess powerful oxidation ability, which can oxidize lipids, proteins and nucleic acids, resulting in serious damage and oxidative stress in cells. Hence, monitoring the concentration of hROS is crucial and can also be accomplished by MOF/AuNCs assemblies. For instance, glutathione-protected AuNCs were encapsulated into ZIF-8 in situ, yielding AuNCs@ZIF-8 nanocomposites with increased fluorescence intensity and lifetime [87]. The fluorescence intensity of AuNCs@ZIF-8 was enhanced approximately ten fold that of GSH–AuNCs, possessing high quantum yield of 11%. Due to the powerful oxidation capacity of hROS, the quenching of fluorescence of AuNCs@ZIF-8 occurred in the presence of ClO^-, based on which ClO^- could be detected in a linear range from 80 nmol/L to 1.0 μmol/L. The detection limit was as low as 30 nmol/L, which was nearly 30-fold lower than that of AuNCs (0.96 μmol/L). Furthermore, due to the efficient cellular internalization, prominent luminescence and

excellent biocompatibility of AuNCs@ZIF-8, bioimaging and detection of endogenous or exogenous hROS in living cells could also be achieved.

Lactose intolerance is a typical genotype related with functional lactose deficiency [88]. Thus, lactose-free products have aroused great interest, promoting the demand to detect trace lactose in relative products. Enzyme cascade amplification is an effective tactic for sensitive sensing [89]. To realize the detection of lactose, AuNCs/β-Gal/GOx@ZIF-8 nanoprobe was fabricated through encapsulation of glucose oxidase (GOx), β-galactosidase (β-Gal) and bovine serum albumin (BSA)-protected AuNCs with ZIF-8 [90]. The nanocomposites showed a prominent emission peak at approximately 650 nm under 375 nm light excitation. Lactose could be firstly decomposed into glucose and galactose by β-Gal. Subsequently, with the aid of enzymatic catalysis of GOx under O_2 present in the air, the generated glucose could be decomposed into H_2O_2 and gluconic acid. Finally, hydroxyl radicals, generated through the reaction between H_2O_2 and Fe^{2+}, could result in the fluorescence quenching of AuNCs/β-Gal/GOx@ZIF-8. Therefore, the detection of lactose in lactose-free milk samples could be achieved. Due to the high local content of the quenching agent and the fluorescent probe in AuNCs/β-Gal/GOx@ZIF-8, the quenching rate was improved to 3.4 times compared to the free AuNCs/β-Gal/GOx system, which was in favor of fast and sensitive sensing. Moreover, a recent study by Feng et al. reported the detection of glucose by GOx–AuNCs@ZIF-8 with the detection limit of 0.30 μmol/L [91].

As a kind of galactose-binding lectin family, galectin-4 participates in the regulation of cell apoptosis and the promotion of cancer metastases, and is overexpressed in some cancers [92]. Consequently, galectin-4 plays important roles as worthy therapeutic targets and potential diagnostic biomarkers for cancer treatment. Based on a similar mechanism mentioned above, a class of fluorescence immunoassay for galectin-4 was proposed by a combination of GOx/ZIF-8 composite and AuNCs–iron(II) system (Fig. 3) [93]. GOx/ZIF-8 was covered by polydopamine (PDA) and then modified by streptavidin (STV) on its surface to selectively combine with the biotinylated antibody against galectin-4. Thus, the concentration of the combined antibody-GOx/ZIF-8–PDA–STV on the galectin-4-presented microplate represents the amount of galectin-4. Glucose could be oxidized to H_2O_2 by GOx, then converted to hydroxyl radical after reaction with iron(II) ions, resulting in the fluorescence quenching of AuNCs. Correspondingly, the detection of galectin-4 could be realized sensitively and the detection limit of galectin-4 was as low as 10 pg/mL.

To eliminate the interference of the false positive signals, ratiometric sensing strategy, which contained two luminescence signals at different wavelengths for built-in self-calibration, was introduced to the platform based on

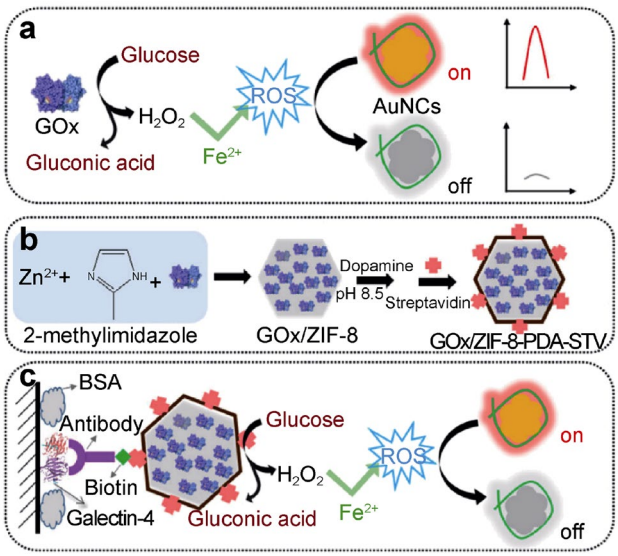

Fig. 3 Schematic diagrams of **a** detection of GOx activity with the AuNCs–iron(II) system, **b** fabrication of the GOx/ZIF-8–PDA–STV complex, and **c** fluorescence immunoassay based on GOx/ZIF-8 and AuNCs–iron(II) system for sensing galectin-4. Reproduced with permission from Ref [93]. Copyright 2017, Springer Nature

MOF/AuNCs assemblies. Dopamine (DA) is an indispensable endogenous neurotransmitter, and the aberrant content of DA in body is highly associated with Alzheimer's, Parkinson's, cardiovascular, schizophrenia disease, etc. [94, 95]. On this point, the accurate detection of DA in complicated biological system is of great importance. Ratiometric assay of DA in intricate biological system was achieved by an innovative dual-emission fluorescence probe, ZIF-8@AuNCs–PFO, which was fabricated by the encapsulation of poly(9,9-dioctylfluorenyl-2,7-diyl) (PFO) dots and AuNCs with ZIF-8 (Fig. 4) [96]. The nanoprobe displayed the emission of PFO at 438 nm and 465 nm, as well as emission of AuNCs at 600 nm. Notably, fluorescence at 600 nm exhibited a prominent enhancement (five-fold increase). In the presence of DA, the fluorescence of AuNCs in ZIF-8@AuNCs–PFO was significantly quenched, while that of PFO dots was nearly unaffected. The fabricated probe showed prominent performance and selectivity for detecting DA against interferential substances within the concentration range of DA from 0.01 to 10,000 μmol/L, and the limit of the detection was as low as 4.8 nmol/L. Recent studies also reported the detection of tetracycline and cephalexin residues in milk with a high sensitivity via a similar methodology based on MOF/AuNCs assemblies [97, 98].

Fluorescence resonance energy transfer (FRET) strategy has also been introduced to MOF/AuNCs assembly-based sensing platform due to its highly sensitive feature and good designability [99, 100]. The short segments of ribonucleic acids (RNA, ca. 20 bases), namely microRNAs, are

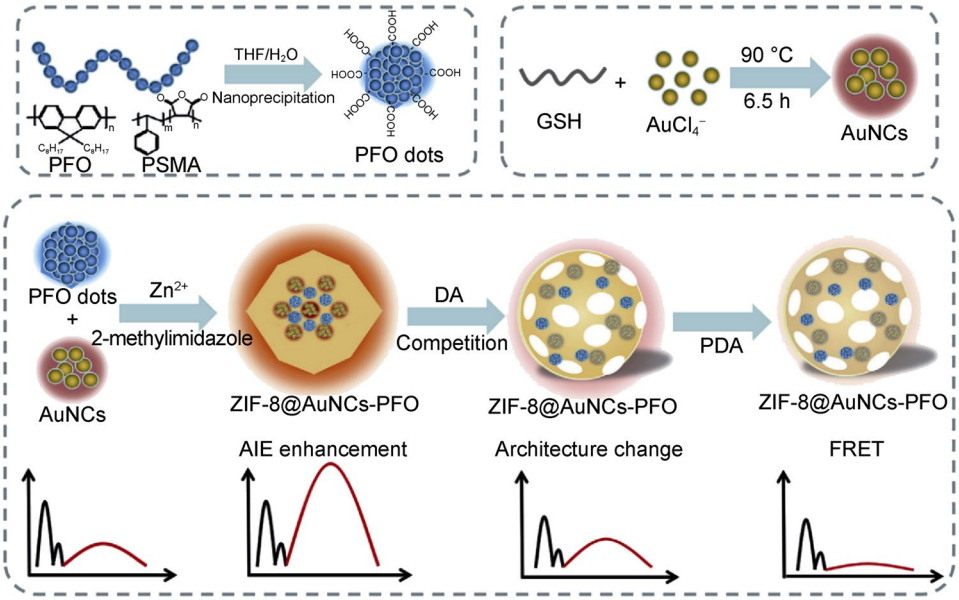

Fig. 4 Schematic representation of ratiometric fluorescence sensing based on ZIF-8@AuNCs–PFO nanoprobe for the detection of DA. Reproduced with permission from Ref [96]. Copyright 2020, Elsevier

key biomarkers highly associated with the cancerization of cells [101, 102]. In consideration of evaluating the status of tumors, identification of epigenetic phenomena and tracking of signaling pathways, it is significant to precisely detect trace contents of intracellular microRNAs in situ. To achieve in vivo therapy and ultrasensitive sensing, a FRET-encoded Zr-MOF@Au-QS/Cy5.5 nanocomposite was constructed by modifying two fluorescent dyes, Cyanine5.5 (Cy5.5) and Quasar (QS), onto the surface of ZrMOF@AuNCs via deoxyribonucleic acid hybridization (Fig. 5) [67]. When encountered with the target intracellular microRNA

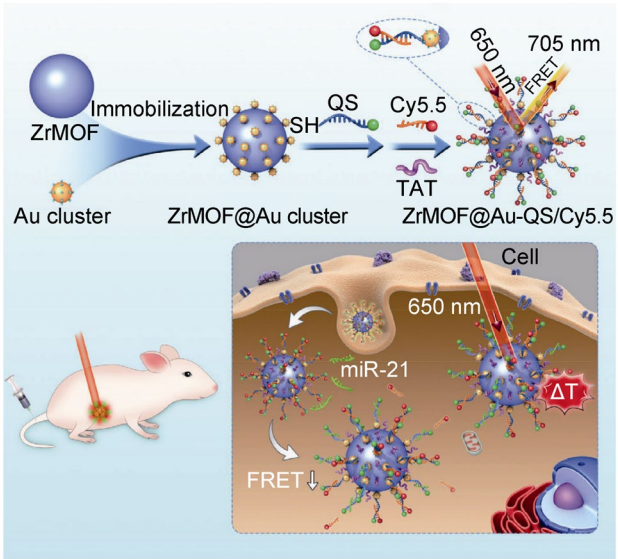

Fig. 5 Schematic diagram of the preparation of Zr-MOF@Au-QS/Cy5.5 probe and miR-21 sensing in living cells and phototherapy monitored by fluorescence imaging in vivo. Reproduced with permission from Ref [67]. Copyright 2021, Wiley–VCH

(miR-21), Cy5.5 would be released from the surface of Zr-MOF@Au-QS/Cy5.5, resulting in the enhancement of fluorescence of QS at 665 nm (F_{665}) and the attenuation of fluorescence of Cy5.5 at 705 nm (F_{705}). With RNA concentration in the range of 0.006 – 67.9 amol/ng, the fluorescence ratio (F_{705}/F_{665}) changed linearly with a detection limit of 4.51 zmol/ng. The ratiometric fluorescence signals and high loading capacity of nucleic acid on the surface of Zr-MOF@AuNCs made it capable of detecting the miR-21 reliably and sensitively. Therefore, the cancer marker miR-21 could be detected in living cells and in vivo by fluorescence imaging. Furthermore, Zr-MOF@Au-QS/Cy5.5 exhibited high photothermal conversion efficiency (53.7%) and could be harnessed for therapeutic purpose in vivo as well. This novel tactic affords new approaches to intelligently quantify miRNAs for simultaneous diagnosis and therapy at the early stage of cancers.

2.2 Metal Ions

The binding of heavy metal ions (e.g., Cu^{2+}, Pb^{2+}, Cd^{2+} and Hg^{2+}) to cellular components can result in change of biological functions, which will induce death or serious diseases [30, 103, 104]. The Environmental Protection Agency (EPA) of the USA has set up a drinking water standard to define the maximum allowed limits of Cu^{2+}, Pb^{2+}, Cd^{2+} and Hg^{2+} as 1.3 (21 000), 0.015 (72), 0.005 (45) and 0.002 (10) ppm (nmol/L), respectively, for their high toxicity. Thus, selectively and sensitively detecting metal ions in complex environmental and biological samples has great significance, and diverse MOF/AuNCs assemblies have been developed for luminescent sensing of metal ions [68, 105–109].

Upon $5d^{10}$-$5d^{10}$ interactions between Au^{+} and Hg^{2+}, the electronic structure of AuNCs changes, causing the fluorescence quenching of AuNCs, which enables the detection of Hg^{2+} based on MOF/AuNCs assemblies [30, 36, 37, 107]. For instance, BSA-protected AuNCs were synthesized in the presence of Zr-MOFs (UiO-66), resulting in the formation of red-emitting AuNCs@UiO-66 with a high quantum yield (11%) [68]. By fluorescence quenching of AuNCs@UiO-66, the detection of Hg^{2+} in real water samples, including tap and river water, could be successfully achieved, with the detection limit of 223 and 193 pmol/L, respectively. In another study, ratiometric fluorescence detection of Hg^{2+} was realized by using CDs/AuNCs@ZIF-8, in which carbon dots (CDs) and AuNCs were co-encapsulated within ZIF-8 [105]. CDs/AuNCs@ZIF-8 inherited the remarkable fluorescence properties of AuNCs and CDs, exhibiting the fluorescence peaks at 640 nm and 440 nm, respectively. Hg^{2+} could quench the fluorescence at 640 nm, while the fluorescence at 440 nm was not affected. The ratio of fluorescence intensity (I_{640}/I_{440}) decreased linearly in the Hg^{2+} concentration range of 3 to 30 nmol/L, with a detection limit of 1 nmol/L. Meanwhile, under 365 nm light irradiation, the fluorescence color of CDs/AuNCs@ZIF-8 changed from red to blue with increasing the concentration of Hg^{2+}, demonstrating the capacity for visual detection of Hg^{2+}. Moreover, Cu^{2+} could also be detected by CDs/AuNCs@ZIF-8 with the detection limit of 0.3 nmol/L [108].

On account of the spatial resolution and excellent sensitivity, single particle-based fluorescence microscopy has been applied to visualize Cu^{2+} [109]. Fluorescent microparticles of AuNCs/ZIF-8 with AuNCs coated on the surface were constructed for visual detection of Cu^{2+} through confocal laser scanning microscopy. Cu^{2+} quenched the fluorescence of AuNCs/ZIF-8 particle within the concentration range from 2 to 15 μmol/L, and the detection limit of Cu^{2+} was 0.9 μmol/L. Significantly, via 3D-reconstructed fluorescence imaging, the distribution of AuNCs and the fluorescence quenching dynamics induced by Cu^{2+} on single AuNCs/ZIF-8 particle could be revealed visually.

Zn^{2+}, an indispensable transition metal ion, takes part in various biological processes of the human body [46]. The aberrant content of Zn^{2+} could result in Alzheimer's disease, stunted growth, chronic inflammation, etc. Therefore, it is important to detect Zn^{2+} in biological samples and food. Recently, Huang and coworkers [106] proposed an interesting strategy to detect Zn^{2+} via in situ formation of AuNCs/ZIF-8. Benefiting from the formation of AuNCs/ZIF-8, the quantum yield of AuNCs could be increased up to 36.6%, almost nine-fold that of the AuNCs. Consequently, a turn-on fluorescent sensor of Zn^{2+} was developed, exhibiting linear range from 12.3 nmol/L to 24.6 μmol/L with the limit of detection as low as 6 nmol/L. The concentration of Zn^{2+} in zinc sulfate syrup oral solution, water, milk, and human serum can be measured successfully via this strategy, which paves a new avenue to detect metal ions based on MOF/AuNCs assemblies.

2.3 Gases and Explosives

The porous properties of MOFs endow the MOF/AuNCs assemblies with the outstanding ability for sensing vapor or gas, since they can concentrate the analytes for the trace detection. Due to the harmful characteristic and odor resembling rotten egg, the noxious hydrogen sulfide (H_2S) could be selectively detected by MOF/AuNCs assemblies upon the strong Au–S interaction and reducibility of H_2S [110]. For instance, Wang and coworkers [69] proposed a novel approach for embedding AuNCs in ZIF-8 via ion-triggered growth. Zn^{2+} induced the precipitation of AuNCs, and then encapsulated in ZIF-8 in the presence of 2-methylimidazole and zinc nitrate (Fig. 6). Interestingly, other metal ions (e.g., Ca^{2+}, Pb^{2+}, Cd^{2+}, Na^{+}, Fe^{3+}, Cu^{2+} and Ni^{2+}) could not trigger this process, as well as non-metal ion precipitator. The resulting AuNCs@ZIF-8 exhibited prolonged lifetime (9.18 μs) and improved quantum yield (33.6%). Furthermore, the selective fluorescence response toward H_2S in gaseous or aqueous phase was achieved successfully based on the fluorescence quenching at 600 nm.

Nitro explosives, for instance, 2,4,6-trinitrophenol (TNP) and 2,4,6-trinitrotoluene (TNT), are generally applied to manufacture landmines for military and industrial applications, and even terrorist activities. In consideration of environmental concerns and homeland security, it is extremely important and urgent to exploit a reliable approach for detecting nitro explosives. AuNCs/ZIF-8 can be used for fast detection of TNT with high sensitivity and selectivity over other explosives (e.g., 1,3,5-trinitro-1,3,5-triazinane (RDX),

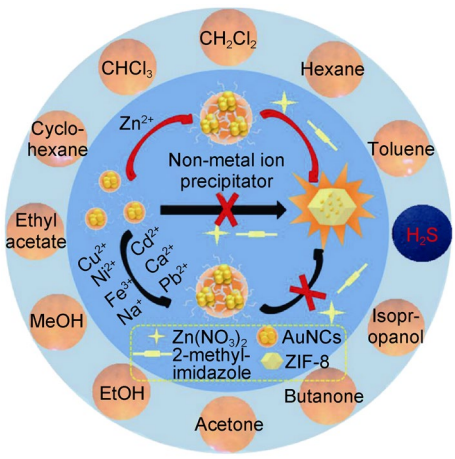

Fig. 6 Schematic depiction of the preparation of AuNCs@ZIF-8 and selective fluorescence detection of H_2S. Reproduced with permission from Ref [69]. Copyright 2018, American Chemical Society

2,4-dinitrotoluene (2,4-DNT), 4-nitrophenol (4-NP) and TNP) [111]. Due to the higher fluorescence intensity, porous structure and the presence of Zn^{2+} as the binding sites, AuNCs/ZIF-8 possesses higher sensitivity for TNT detection than AuNCs, as evidenced by the shortened lifetime after fluorescence quenching by TNT. The fluorescence quenching is likely caused by the photoinduced electron transfer from the excited AuNCs/ZIF-8 to the electron-deficient TNT. The detection limit of TNT is 5 nmol/L, and the response of explosive takes place rapidly within 1 min.

3 Colorimetric Sensing

By monitoring the color variation of the solution, detection of target analytes can be facilely achieved via colorimetric sensing, which possesses excellent portability and economic efficiency. In recent years, on account of the characteristics of ultrasmall sizes, high fraction of surface atoms, distinct electronic structure, and well-defined compositions, AuNCs have been proved to possess strong enzyme-like catalytic activity, making them promising for colorimetric sensing [103, 112]. Benefiting from integration with MOFs, many characteristics of AuNCs, such as stability and catalytic capacity, can be further greatly improved [113–120]. In addition, the integration can endow the assemblies with intelligent responsiveness and the opportunity of developing enzyme cascade amplification strategy. These outstanding performances of MOF/AuNCs assemblies facilitate the sensitive colorimetric sensing of organophosphorus pesticides (OPs), acetylcholinesterase (AChE), choline oxidase (CHO), glucose, hydrogen peroxide, etc. [70, 71, 121–123].

In 2020, Wu et al. [71] proposed an innovative strategy realizing the enzyme-mimicking catalysis of well-defined AuNCs for the first time. Based on host–guest chemistry, they combined rigid and water-soluble γ-CD-MOF with well-defined AuNCs protected by lipophilic ligands adamantanethiolate (Au_{40}(S-Adm)$_{22}$) (Fig. 7). Interestingly, the resulted assemblies exhibited outstanding water solubility and horseradish peroxidase (HRP)-like activity, which were distinctive from the primitive Au_{40}(S-Adm)$_{22}$ NCs. Importantly, with the aid of density functional theory calculation, an elaborate HRP-mimicking catalysis mechanism was also revealed. These remarkable outcomes provide guidance for the future design and application of metal NCs in colorimetric sensing.

With regard to biological nerve conduction activity, AChE is a type of vital important enzymes and can serve as biomarkers to be extensively applied in biosensing and diagnosis areas [124]. Nevertheless, the widely used pesticides, organophosphorus compounds, could inhibit AChE in the body, resulting in irreversible damages in the nervous system [125, 126]. Consequently, it is highly urgent to develop an extremely sensitive and simple biosensor for the monitoring of the AChE activity and trace organophosphorus pesticides. Liu and coworkers [70] packaged AuNCs into ZIF-8, then accomplished the combination of colorimetric and fluorescence sensing via the enzyme cascade amplification strategy (Fig. 8). Under the cascaded enzymolysis of AChE and choline oxidase (CHO), acetylcholine (ACh) was hydrolyzed to generate H_2O_2. On the one hand, H_2O_2 destroyed ZIF-8 to impair the enhancement effect on the fluorescence of AuNCs, and then the fluorescence intensity declined gradually. On the other hand, H_2O_2 acted as a substrate, and the dissociated AuNCs with HRP-mimic catalytic activity enabled the oxidization of colorless 3,3′,5,5′-tetramethylbenzidine (TMB) to blue-colored oxTMB. Consequently, a

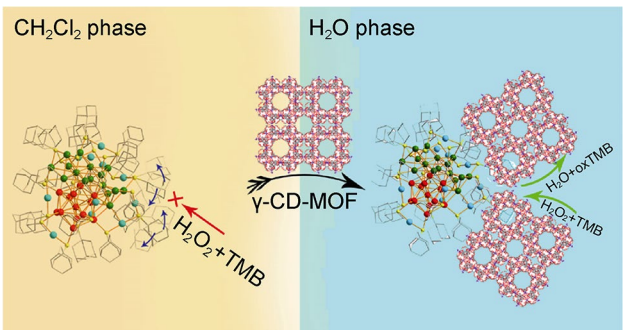

Fig. 7 Schematic diagram of fabricating water-soluble Au_{40}/γ-CD-MOF for enzyme-like catalysis. Reproduced with permission from Ref [71]. Copyright 2020, American Chemical Society

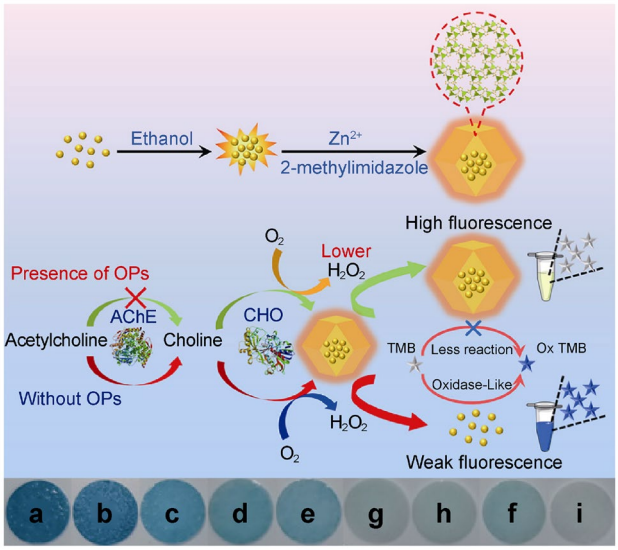

Fig. 8 Schematic illustration of the mechanism for sensing OPs and photographs of colorimetric paper strips in the presence of diverse contents of OPs (from a to i: 0, 0.00075, 0.0015, 0.015, 0.15, 1.5, 7.5, 15, 30 mg/L). Reproduced with permission from Ref [70]. Copyright 2021, American Chemical Society

fluorescence-colorimetric double-signal biosensor was set up based on the restriction of AChE activity by organophosphorus pesticides. Furthermore, by virtue of the fluorescence intensity variation of AuNCs@ZIF-8 and color variation of TMB, a fluorescence-colorimetric dual-signal determination of organophosphorus pesticides was accomplished on the basis of colorimetric paper strips. To enable the real-time monitoring of insecticide pollution in a more accurate way, a smartphone APP was designed by the identification of the gray value of the solution color. The on-site detection limit of organophosphorus pesticides was 0.4 μg/L.

Diabetes has been regarded as a kind of serious metabolic illness injuring the nerves, heart, kidneys and eyes. Detection of glucose is critical for the mechanism study of glucose metabolism, and the timely diagnosis of diabetes, which can greatly improve the therapeutic effect. The enzyme cascade of HRP and GOx has been extensively applied to the detection of glucose, and the detection is sensitive and selective benefiting from the specific catalysis on glucose by GOx [127]. For example, BSA-protected AuNCs and GOx were encapsulated by ZIF-8, which could sensitively and selectively detect glucose via colorimetric sensing on the basis of cascade reaction [121]. Under the enzymolysis of GOx, glucose was decomposed to gluconic acid accompanied with H_2O_2 generation, which acted as a substrate for HRP-mimicking catalysis of AuNCs to oxidize colorless TMB to blue oxTMB with an absorption peak at 652 nm. Compared with free GOx/AuNCs, the catalytic activity of GOx&AuNCs@ZIF-8 was improved by over 19-fold, which was mainly attributed to the cascade reaction and protection of enzymes by ZIF-8 coating. This glucose sensor exhibited a linear range of 1.0−25.0 mmol/L and a detection limit of 0.8 mmol/L. Moreover, benefiting from the shielding effect of the ZIF-8 shell, GOx&AuNCs@ZIF-8 exhibited excellent stability in the presence of chelating compounds and digesting enzymes, and also good long-term storage stability.

4 Electrochemiluminescence (ECL) Sensing

ECL is a kind of energy-relaxation process induced by an energetic electron-transfer reaction. With distinct advantages such as excellent controllability, low cost and inherent low background, ECL has aroused extensive attentions as an effective analytical means for sensing [4, 128]. Recent studies showed that AuNCs possess attractive ECL performance due to their interactions with highly reactive radical species produced by the electrochemical process [77, 129]. Upon coordination-assisted self-assembly, the porous structure of MOFs can not only enhance the electrochemical excitation and reduce the self-quenching effect of AuNCs, but also restrain the energy dissipation triggered by rotation and vibration of ligand to impede nonradiative transition of AuNCs as well. These features endow MOF/AuNCs assemblies with enhanced ECL efficiency which is favorable for ECL sensing [72, 73].

Yuan et al. [72] first reported the outstanding anodic ECL performance of GSH–AuNCs@ZIF-8 in the presence of coreactant (triethylamine, TEA), where the ECL intensity of GSH–AuNCs@ZIF-8 was increased to nearly ten times that of AuNCs (Fig. 9). Accordingly, a "signal off" sensing platform was proposed for the detection of rutin, which was widely applied for antitumor, antiinflammatory and antiviral activities [130]. The ECL quenching mechanism was proposed to be related with the inhibition of the excited-state species generation and annihilation of the excited-state species by rutin. The sensing of rutin is convenient, fast responsive and ultrasensitive with the detection limit of 10 nmol/L. In another study, Omidfar and coworkers [73] exploited a sandwich paper-based ECL biosensor based on Zr-MOF/Fe_3O_4/AuNCs nanocomposite for detecting glycated hemoglobin (HbA1c), a famous biomarker for clinically diagnosing diabetes [131, 132]. Anti-HbA1c monoclonal antibody was labeled by Zr-MOF/Fe_3O_4/AuNCs as the tracing probe, and reduced graphene oxide (rGO) was used as the immobilization platform of sensing element. HbA1c was sensitively and selectively detected by antibody-labeled Zr-MOF/Fe_3O_4/AuNCs due to its remarkable capacity to selectively snatch HbA1c from human blood sample. The linear response concentration of HbA1c ranged from 2 to 18%, and the detection limit of HbA1c was as low as 0.072%. This paper-based screen-printed ECL biosensor possesses the merit of a wide linear range, low detection limit, short assay time, and remarkable selectivity, which holds great potential for further high-performance biosensing.

5 (Photo)Electrochemical Sensing

Due to the merits of high sensitivity, low cost and easy operation, electrochemical sensing has been proved to be a powerful tool for biological diagnosis, environmental monitoring, food safety administration, etc. [133–135]. Highly sensitive electrochemical sensors based on MOF/AuNCs assemblies have been exploited as well in recent years. For instance, Du and Zhang et al. [75] encapsulated AuNCs into a kind of Zr-MOF (521-MOF) for the detection of cocaine, which is an important analyte in law enforcement and clinical diagnostics (Fig. 10). The fabricated 2D AuNCs@521-MOF nanosheets possess many characteristics, such as remarkable biocompatibility, good electrochemical activity, and high specific surface area. In addition, they can strongly bind to biomolecule-bearing phosphate groups, which facilitates attachment of cocaine aptamer strands onto 2D AuNCs@521-MOF-modified substrate. Consequently, cocaine can be detected based on its specific binding to

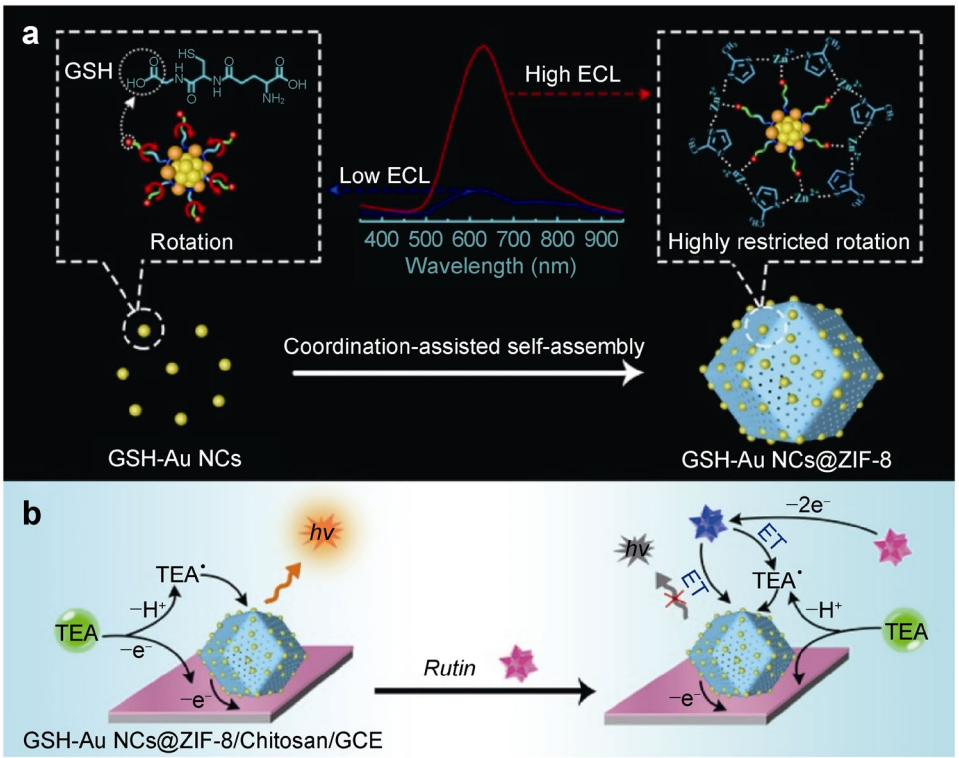

Fig. 9 **a** Schematic diagram of fabricating GSH–AuNCs@ZIF-8 through ECL-enhanced mechanism and coordination-assisted self-assembly strategy; **b** ECL turn-off strategy for sensing rutin via the GSH–AuNCs@ZIF-8/TEA system. Reproduced with permission from Ref [72]. Copyright 2021, American Chemical Society

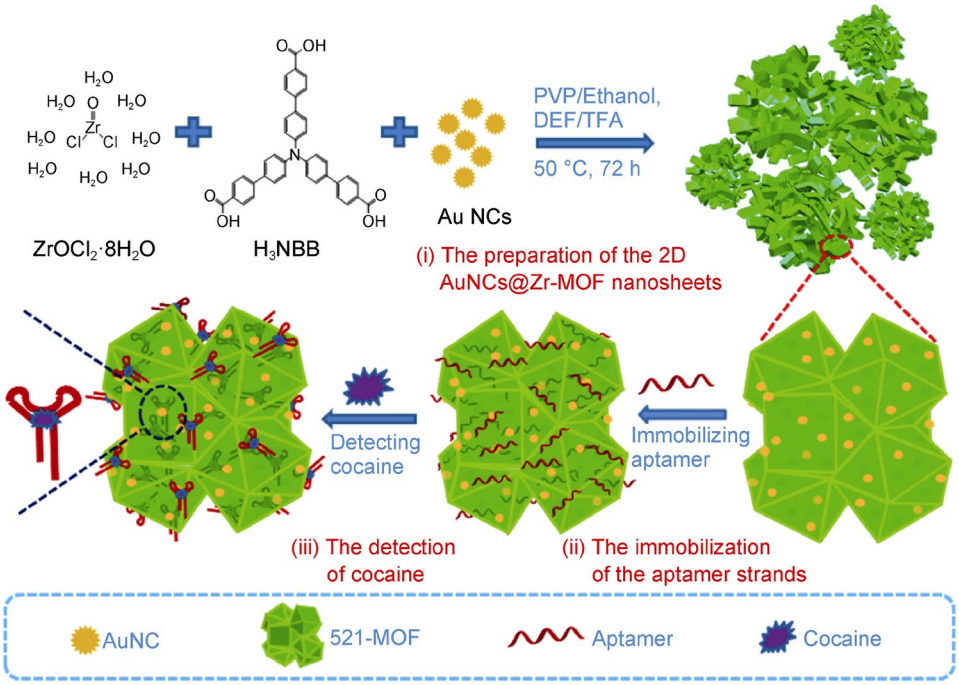

Fig. 10 Schematic representation of construction of electrochemical biosensing via AuNCs@Zr-MOF nanosheets for sensing cocaine, involving (i) fabrication of 2D AuNCs@Zr-MOF nanosheets, (ii) immobilization of the aptamer strands, and (iii) sensing of cocaine. Reproduced with permission from Ref [75]. Copyright 2017, American Chemical Society

cocaine aptamer strands. The 2D AuNCs@521-MOF-based aptasensor can detect trace cocaine sensitively and selectively with the linear concentration range from 0.001 to 1.0 ng/mL. The detection limit of cocaine is 2.22 pmol/L (0.75 pg/mL) identified by differential pulse voltammetry and 1.29 pmol/L (0.44 pg/mL) by electrochemical impedance spectroscopy. This aptasensor exhibits merits of good applicability, stability, repeatability and high selectivity.

Interferon-gamma (IFN-γ) is a significant cytokine generated by immune cells in the presence of intracellular

pathogens, which is regarded as the major mediator for activation of human macrophage's antimicrobial activity [136]. Abnormal IFN-γ expression can result in abnormity of cell development and function, for instance, aberrant differentiation of natural killer cell and apoptosis of hematopoietic stem cell. Therefore, it is extremely significant to sensitively detect IFN-γ in clinical therapeutics and diagnosis. Wang and coworkers [74] reported an innovative electrochemical biosensor based on AuNCs-anchored graphene@ZIF-8 (AuNCs–GR@ZIF-8) for ultrasensitively detecting IFN-γ. AuNCs–GR@ZIF-8 was modified on the glassy carbon electrode (GCE) for anchoring capture probe and mercapto-1-hexanol. Since recognition DNA (R-DNA) can specifically recognize IFN-γ, the double-stranded DNA composed of R-DNA and triggered DNA (T-DNA) can be unwound in the presence of IFN-γ. The dissociated T-DNA combined with capture probe on the electrode, inducing layered-branched hybridization chain reaction (LB-HCR) with the cascade-like assembly of four hairpins. IFN-γ activated LB-HCR process and triggered the integration of in situ formed dendritic DNA nanostructures with hemin/G-quadruplex DNAzyme, which acted as an amplifying label. With thionine as the electron mediator, the output of the amplified signal was achieved by hemin/G-quadruplex DNAzyme catalyzed H_2O_2 reduction. The multiple-amplified strategy possessed excellent analytical capacity towards IFN-γ over a broad linear range of 1 fmol/L−50 pmol/L with the detection limit of 0.6 fmol/L.

To improve the photoelectrochemical (PEC) performance and photo-to-current conversion efficiency, MOFs based on Mg and 3,4,9,10-perylene tetracarboxylic acid was synthesized [76]. The resulting Mg–PTCA MOFs, as an outstanding photoelectric material, were coated onto the electrode. AuNCs were used as the quencher, which could be seized by the capture DNA on the electrode. Then, with target-triggered three-dimensional DNA scaffold (3D-Sca) as the signal amplifier, a regenerated biosensor was achieved for detecting microRNA (miRNA-21). The miRNA 21 could be detected sensitively over the dynamic range of 10 amol/L to 10 pmol/L and the limit of detection is 2.8 amol/L. The biosensor also exhibited excellent analytical performance in nuclear extraction of different cancer cells, suggesting the potential for accurate prognostic judgment and early diagnosis for diseases.

6 Summary and Outlook

In recent years, MOF/AuNCs assemblies have attracted extensive attention in sensing due to their remarkable properties. In this review, we have comprehensively summarized recent advances of MOF/AuNCs assemblies in sensing fields. The marriage of MOFs with AuNCs endows MOF/AuNCs assemblies with enhanced optical and electrochemical properties, which are in favor of developing highly sensitive and selective sensors. Various sensing strategies have been discussed, including luminescence sensing, colorimetric sensing, electrochemiluminescence sensing, electrochemical and photoelectrochemical sensing. To meet the demand of various sensing applications, diverse ligands have been designed to modulate the properties of AuNCs, such as adamantanethiolate, glutathione, proteins, and peptides. Particularly, different types of MOFs have been combined with AuNCs due to their distinct features, including ZIFs (e.g., ZIF-8), CD-MOFs (e.g., γ-CD-MOF), MILs (e.g. NH_2-MIL-101(Fe)), Zr-MOFs (e.g., UiO-66, PCN-224, 521-MOF), and Mg–PTCA MOFs. As outlined here, many outstanding MOF/AuNCs assemblies have been exploited for sensing biomolecules (e.g., caspase-3, HbA1c, IFN-γ, microRNA, galectin-4, lactose, Cys, glucose, ROS, rutin, DA), small molecules (e.g., pesticides, H_2O_2), metal ions (e.g., Hg^{2+}, Cu^{2+}, Zn^{2+}), gases (e.g., H_2S), explosives (e.g., TNT), etc.

Although enormous success in sensing based on MOF/AuNCs assemblies has been achieved, some challenges still remain to be dealt with. Firstly, efforts will be worthwhile to expand the scope of detectable analytes, such as bacteria [137], virus (e.g., coronavirus COVID-19) [138], volatile organic compounds (e.g., aliphatic and aromatic hydrocarbons, aldehydes) and toxic gases (e.g., NH_3, SO_2, NO_x, CS_2) [60]. Secondly, the integration of MOFs with ultrasmall-sized AuNCs provides great opportunities for sensing application beyond the present advances, which have not been exploited adequately yet. For instance, integrating multiple sensing elements into one platform enables sensing different analytes simultaneously, which is very important for discrimination of cancer cells, proteins and bacteria. In addition, the atomically precise structure of AuNCs makes it possible to deeply understand the structure–property correlation of these assemblies, which can further guide the precise construction of custom-designed MOF/AuNCs composites for better sensing applications. Therefore, it is of great importance to exploit efficient strategies to get single crystals of these MOFs-mediated AuNCs, such as solvent evaporation, hydrothermal method, and electrocrystallization. Thirdly, efforts should be devoted to couple two or more signaling modes by rational design of MOF/AuNCs assemblies, which will enable the development of multimode sensors, such as luminescence–electricity and luminescence–ferroelectricity. Fourthly, the integration of sensing with therapy has been preliminarily explored, but there is still room for expanding advanced biomedical applications based on MOF/AuNCs assemblies by combining sensing with therapy. Finally, development of portable diagnostic devices based on MOF/AuNCs assemblies is still in its early stage, but of great importance [139], and can be achieved by

taking the remarkable processibility of MOFs into account in the future [61].

Overall, MOF/AuNCs assemblies have shown great potential for sensing application in recent years due to their multiple advantages. Although there are still some challenges to be addressed, impressive advances made by scientists have offered important foundation for the fabrication of high-performance sensing systems. Advance in this fast-growing field will doubtlessly contribute to generating innovative materials for advanced sensing in the near future.

Acknowledgements This work was supported by the Natural Science Foundation of Chongqing (cstc2020jcyj-msxmX1053) and the Research Fund of the State Key Laboratory of Solidification Processing (NPU), China (2020-QZ-01).

Declarations

Conflict of interest The authors declare no conflicts of interests.

References

1. Wu J, Wang X, Wang Q, Lou Z, Li S, Zhu Y, Qin L, Wei H. Nanomaterials with enzyme-like characteristics (nanozymes): next-generation artificial enzymes (II). Chem Soc Rev. 2019;48(4):1004–76.
2. Zheng K, Setyawati MI, Leong DT, Xie J. Antimicrobial silver nanomaterials. Coord Chem Rev. 2018;357:1–17.
3. Song N, Yang Y-W. Molecular and supramolecular switches on mesoporous silica nanoparticles. Chem Soc Rev. 2015;44(11):3474–504.
4. Tan LL, Wei M, Shang L, Yang YW. Cucurbiturils-mediated noble metal nanoparticles for applications in sensing, SERS, theranostics, and catalysis. Adv Funct Mater. 2021;31(1):2007277.
5. Chen PC, Periasamy AP, Harroun SG, Wu WP, Chang HT. Photoluminescence sensing systems based on copper, gold and silver nanomaterials. Coord Chem Rev. 2016;320:129–38.
6. Shang L, Dong S, Nienhaus GU. Ultra-small fluorescent metal nanoclusters: synthesis and biological applications. Nano Today. 2011;6(4):401–18.
7. Chakraborty I, Pradeep T. Atomically precise clusters of noble metals: emerging link between atoms and nanoparticles. Chem Rev. 2017;117(12):8208–71.
8. Kang X, Zhu M. Metal nanoclusters stabilized by selenol ligands. Small. 2019;15(43):1902703.
9. Zheng J, Nicovich PR, Dickson RM. Highly fluorescent noble-metal quantum dots. Annu Rev Phys Chem. 2007;58(1):409–31.
10. Zhang L, Wang E. Metal nanoclusters: new fluorescent probes for sensors and bioimaging. Nano Today. 2014;9(1):132–57.
11. Jin R. Atomically precise metal nanoclusters: stable sizes and optical properties. Nanoscale. 2015;7(5):1549–65.
12. Casteleiro B, Martinho JMG, Farinha JPS. Encapsulation of gold nanoclusters: stabilization and more. Nanoscale. 2021;13:17199–217.
13. Kang X, Zhu M. Intra-cluster growth meets inter-cluster assembly: the molecular and supramolecular chemistry of atomically precise nanoclusters. Coord Chem Rev. 2019;394:1–38.
14. Guan ZJ, Hu F, Li JJ, Wen ZR, Lin YM, Wang QM. Isomerization in alkynyl-protected gold nanoclusters. J Am Chem Soc. 2020;142(6):2995–3001.
15. Wang QY, Wang J, Wang S, Wang ZY, Cao M, He CL, Yang JQ, Zang SQ, Mak TCW. O-carborane-based and atomically precise metal clusters as hypergolic materials. J Am Chem Soc. 2020;142(28):12010–4.
16. Wen M, Li Y, Zhong W, Li Q, Cao L, Tan LL, Shang L. Interactions of cationic gold nanoclusters with serum proteins and effects on their cellular responses. J Colloid Interface Sci. 2022;610:116–25.
17. Kang X, Li Y, Zhu M, Jin R. Atomically precise alloy nanoclusters: syntheses, structures, and properties. Chem Soc Rev. 2020;49(17):6443–514.
18. Hulkko E, Lopez-Acevedo O, Koivisto J, Levi-Kalisman Y, Kornberg RD, Pettersson M, Häkkinen H. Electronic and vibrational signatures of the Au_{102}(p-MBA)$_{44}$ cluster. J Am Chem Soc. 2011;133(11):3752–5.
19. Wu Z. Anti-galvanic reduction of thiolate-protected gold and silver nanoparticles. Angew Chem Int Ed. 2012;51(12):2934–8.
20. Zhu M, Aikens CM, Hendrich MP, Gupta R, Qian H, Schatz GC, Jin R. Reversible switching of magnetism in thiolate-protected Au_{25} superatoms. J Am Chem Soc. 2009;131(7):2490–2.
21. Gautier C, Bürgi T. Chiral n-isobutyryl-cysteine protected gold nanoparticles: preparation, size selection, and optical activity in the UV−vis and infrared. J Am Chem Soc. 2006;128(34):11079–87.
22. Varnavski O, Ramakrishna G, Kim J, Lee D, Goodson T. Critical size for the observation of quantum confinement in optically excited gold clusters. J Am Chem Soc. 2010;132(1):16–7.
23. Shang L, Brandholt S, Stockmar F, Trouillet V, Bruns M, Nienhaus GU. Effect of protein adsorption on the fluorescence of ultrasmall gold nanoclusters. Small. 2012;8(5):661–5.
24. Chen D, Luo Z, Li N, Lee JY, Xie J, Lu J. Amphiphilic polymeric nanocarriers with luminescent gold nanoclusters for concurrent bioimaging and controlled drug release. Adv Funct Mater. 2013;23(35):4324–31.
25. Zhao J, Jin R. Heterogeneous catalysis by gold and gold-based bimetal nanoclusters. Nano Today. 2018;18:86–102.
26. Luo Z, Yuan X, Yu Y, Zhang Q, Leong DT, Lee JY, Xie J. From aggregation-induced emission of Au(I)–thiolate complexes to ultrabright Au(0)@Au(I)–thiolate core–shell nanoclusters. J Am Chem Soc. 2012;134(40):16662–70.
27. Liu L, Corma A. Metal catalysts for heterogeneous catalysis: from single atoms to nanoclusters and nanoparticles. Chem Rev. 2018;118(10):4981–5079.
28. Zhong W, Wen M, Xu J, Wang H, Tan LL, Shang L. Simultaneous regulation of optical properties and cellular behaviors of gold nanoclusters by pre-engineering the biotemplates. Chem Commun. 2020;56(77):11414–7.
29. Xu J, Shang L. Emerging applications of near-infrared fluorescent metal nanoclusters for biological imaging. Chin Chem Lett. 2018;29(10):1436–44.
30. Chen LY, Wang CW, Yuan Z, Chang HT. Fluorescent gold nanoclusters: recent advances in sensing and imaging. Anal Chem. 2015;87(1):216–29.
31. Halawa MI, Lai J, Xu G. Gold nanoclusters: synthetic strategies and recent advances in fluorescent sensing. Mater Today Nano. 2018;3:9–27.
32. Cifuentes-Rius A, Deepagan VG, Xie J, Voelcker NH. Bright future of gold nanoclusters in theranostics. ACS Appl Mater Interfaces. 2021;13(42):49581–8.
33. Wang L, Hou Q, Zheng W, Jiang X. Fluorescent and antibacterial aminobenzeneboronic acid (ABA)-modified gold nanoclusters for self-monitoring residual dosage and smart wound care. ACS Nano. 2021;15(11):17885–94.
34. Zheng K, Xie J. Cluster materials as traceable antibacterial agents. Acc Mater Res. 2021;2(11):1104–16.

35. Li Y, Zhen J, Tian Q, Shen C, Zhang L, Yang K, Shang L. One step synthesis of positively charged gold nanoclusters as effective antimicrobial nanoagents against multidrug-resistant bacteria and biofilms. J Colloid Interface Sci. 2020;569:235–43.
36. Xu J, Li J, Zhong W, Wen M, Sukhorukov G, Shang L. The density of surface ligands regulates the luminescence of thiolated gold nanoclusters and their metal ion response. Chin Chem Lett. 2021;32(8):2390–4.
37. Shang L, Yang L, Stockmar F, Popescu R, Trouillet V, Bruns M, Gerthsen D, Nienhaus GU. Microwave-assisted rapid synthesis of luminescent gold nanoclusters for sensing Hg^{2+} in living cells using fluorescence imaging. Nanoscale. 2012;4(14):4155–60.
38. Chen Y, Li L, Gong L, Zhou T, Liu J. Surface regulation towards stimuli-responsive luminescence of ultrasmall thiolated gold nanoparticles for ratiometric imaging. Adv Funct Mater. 2019;29(10):1806945.
39. Xu S, Gao T, Feng X, Fan X, Liu G, Mao Y, Yu X, Lin J, Luo X. Near infrared fluorescent dual ligand functionalized Au NCs based multidimensional sensor array for pattern recognition of multiple proteins and serum discrimination. Biosens Bioelectron. 2017;97:203–7.
40. Shang L, Stockmar F, Azadfar N, Nienhaus GU. Intracellular thermometry by using fluorescent gold nanoclusters. Angew Chem Int Ed. 2013;52(42):11154–7.
41. Yang H, Lu F, Sun Y, Yuan Z, Lu C. Fluorescent gold nanocluster-based sensor array for nitrophenol isomer discrimination via an integration of host–guest interaction and inner filter effect. Anal Chem. 2018;90(21):12846–53.
42. Li D, Kumari B, Makabenta JM, Gupta A, Rotello V. Effective detection of bacteria using metal nanoclusters. Nanoscale. 2019;11(46):22172–81.
43. Tao Y, Lin Y, Huang Z, Ren J, Qu X. Incorporating graphene oxide and gold nanoclusters: a synergistic catalyst with surprisingly high peroxidase-like activity over a broad pH range and its application for cancer cell detection. Adv Mater. 2013;25(18):2594–9.
44. Tan LL, Li H, Qiu YC, Chen DX, Wang X, Pan RY, Wang Y, Zhang SXA, Wang B, Yang YW. Stimuli-responsive metal–organic frameworks gated by pillar[5]arene supramolecular switches. Chem Sci. 2015;6(3):1640–4.
45. Tan LL, Song N, Zhang SXA, Li H, Wang B, Yang YW. Ca^{2+}, pH and thermo triple-responsive mechanized Zr-based MOFs for on-command drug release in bone diseases. J Mater Chem B. 2016;4(1):135–40.
46. Tan LL, Li H, Zhou Y, Zhang Y, Feng X, Wang B, Yang YW. Zn^{2+}-triggered drug release from biocompatible zirconium MOFs equipped with supramolecular gates. Small. 2015;11(31):3807–13.
47. Hao YC, Chen LW, Li J, Guo Y, Su X, Shu M, Zhang Q, Gao WY, Li S, Yu ZL, Gu L, Feng X, Yin AX, Si R, Zhang Y, Wang B, Yan CH. Metal–organic framework membranes with single-atomic centers for photocatalytic CO_2 and O_2 reduction. Nat Commun. 2021;12(1):2682.
48. Yu H, Wu X, Mu Q, Wei Z, Gu Y, Yuan X, Lu Y, Deng Z, Peng Y. Robust photocatalytic hydrogen production on metal–organic layers of Al-TCPP with ultrahigh turnover numbers. Chin Chem Lett. 2021;32(12):3833–6.
49. Chen KJ, Madden DG, Mukherjee S, Pham T, Forrest KA, Kumar A, Space B, Kong J, Zhang QY, Zaworotko MJ. Synergistic sorbent separation for one-step ethylene purification from a four-component mixture. Science. 2019;366(6462):241–6.
50. Li J, Wang J, Li Q, Zhang M, Li J, Sun C, Yuan S, Feng X, Wang B. Coordination polymer glasses with lava and healing ability for high-performance gas sieving. Angew Chem Int Ed. 2021;60(39):21304–9.
51. Zhou J, Wang B. Emerging crystalline porous materials as a multifunctional platform for electrochemical energy storage. Chem Soc Rev. 2017;46(22):6927–45.
52. Kong L, Zhong M, Shuang W, Xu Y, Bu X-H. Electrochemically active sites inside crystalline porous materials for energy storage and conversion. Chem Soc Rev. 2020;49(8):2378–407.
53. Stavila V, Talin AA, Allendorf MD. MOF-based electronic and opto-electronic devices. Chem Soc Rev. 2014;43(16):5994–6010.
54. Lustig WP, Li J. Luminescent metal–organic frameworks and coordination polymers as alternative phosphors for energy efficient lighting devices. Coord Chem Rev. 2018;373:116–47.
55. Yin HQ, Yin XB. Metal–organic frameworks with multiple luminescence emissions: designs and applications. Acc Chem Res. 2020;53(2):485–95.
56. Li E, Jie K, Liu M, Sheng X, Zhu W, Huang F. Vapochromic crystals: understanding vapochromism from the perspective of crystal engineering. Chem Soc Rev. 2020;49(5):1517–44.
57. Dong R, Han P, Arora H, Ballabio M, Karakus M, Zhang Z, Shekhar C, Adler P, Petkov PS, Erbe A, Mannsfeld SCB, Felser C, Heine T, Bonn M, Feng X, Cánovas E. High-mobility band-like charge transport in a semiconducting two-dimensional metal–organic framework. Nat Mater. 2018;17(11):1027–32.
58. Sun S, Fan Y, Du J, Song Z, Zhao H. CNT-modified MIL-88(NH_2)-Fe for enhancing DNA-regulated peroxidase-like activity. J Anal Test. 2019;3(3):238–45.
59. Hu L, Dai C, Chen L, Zhu Y, Hao Y, Zhang Q, Gu L, Feng X, Yuan S, Wang L, Wang B. Metal-triazolate-framework-derived FeN_4Cl_1 single-atom catalysts with hierarchical porosity for the oxygen reduction reaction. Angew Chem Int Ed. 2021;60(52):27324–9.
60. Li HY, Zhao SN, Zang SQ, Li J. Functional metal–organic frameworks as effective sensors of gases and volatile compounds. Chem Soc Rev. 2020;49(17):6364–401.
61. Feng YY, Wang YX, Ying YB. Structural design of metal–-organic frameworks with tunable colorimetric responses for visual sensing applications. Coord Chem Rev. 2021;446: 214102.
62. Kaur M, Kumar S, Yusuf M, Lee J, Brown RJC, Kim KH, Malik AK. Post-synthetic modification of luminescent metal–organic frameworks using Schiff base complexes for biological and chemical sensing. Coord Chem Rev. 2021;449: 214214.
63. Kukkar P, Kim K-H, Kukkar D, Singh P. Recent advances in the synthesis techniques for zeolitic imidazolate frameworks and their sensing applications. Coord Chem Rev. 2021;446: 214109.
64. Zhou X, Li J, Tan LL, Li Q, Shang L. Novel perylene probe-encapsulated metal–organic framework nanocomposites for ratiometric fluorescence detection of ATP. J Mater Chem B. 2020;8(16):3661–6.
65. Yin X, Yang B, Chen B, He M, Hu B. Multifunctional gold nanocluster decorated metal–organic framework for real-time monitoring of targeted drug delivery and quantitative evaluation of cellular therapeutic response. Anal Chem. 2019;91(16):10596–603.
66. Cai Y, Hua Y, Yin M, Liu H, Li S, Wang F, Wang H. Fabrication of test strips with gold-silver nanospheres and metal–organic frameworks: a fluorimetric method for sensing trace cysteine in hela cells. Sensor Actuat B. 2020;302: 127198.
67. Liang Z, Hao C, Chen C, Ma W, Sun M, Xu L, Xu C, Kuang H. Ratiometric FRET encoded hierarchical ZrMOF@Au cluster for ultrasensitive quantifying microRNA in vivo. Adv Mater. 2021;34:2107449.
68. Govindaraju S, Puthiaraj P, Lee MH, Yun K. Photoluminescent AuNCs@UiO-66 for ultrasensitive detection of mercury in water samples. ACS Omega. 2018;3(9):12052–9.
69. Gao Q, Xu S, Guo C, Chen Y, Wang L. Embedding nanocluster in MOF via crystalline ion-triggered growth strategy for improved

emission and selective sensing. ACS Appl Mater Interfaces. 2018;10(18):16059–65.
70. Cai Y, Zhu H, Zhou W, Qiu Z, Chen C, Qileng A, Li K, Liu Y. Capsulation of AuNCs with AIE effect into metal–organic framework for the marriage of a fluorescence and colorimetric biosensor to detect organophosphorus pesticides. Anal Chem. 2021;93(19):7275–82.
71. Zhao Y, Zhuang S, Liao L, Wang C, Xia N, Gan Z, Gu W, Li J, Deng H, Wu Z. A dual purpose strategy to endow gold nanoclusters with both catalysis activity and water solubility. J Am Chem Soc. 2020;142(2):973–7.
72. Nie Y, Tao X, Zhang H, Chai YQ, Yuan R. Self-assembly of gold nanoclusters into a metal–organic framework with efficient electrochemiluminescence and their application for sensitive detection of rutin. Anal Chem. 2021;93(7):3445–51.
73. Ahmadi A, Khoshfetrat SM, Kabiri S, Dorraji PS, Larijani B, Omidfar K. Electrochemiluminescence paper-based screen-printed electrode for HbA1c detection using two-dimensional zirconium metal–organic framework/Fe_3O_4 nanosheet composites decorated with Au nanoclusters. Microchim Acta. 2021;188(9):296.
74. Bao T, Wen M, Wen W, Zhang X, Wang S. Ultrasensitive electrochemical biosensor of interferon-gamma based on gold nanoclusters-graphene@zeolitic imidazolate framework-8 and layered-branched hybridization chain reaction. Sens Actuat B. 2019;296: 126606.
75. Su F, Zhang S, Ji H, Zhao H, Tian JY, Liu CS, Zhang Z, Fang S, Zhu X, Du M. Two-dimensional zirconium-based metal organic framework nanosheet composites embedded with Au nanoclusters: a highly sensitive electrochemical aptasensor toward detecting cocaine. ACS Sens. 2017;2(7):998–1005.
76. Mo F, Han Q, Chen M, Meng H, Guo J, Fu Y. Novel optoelectronic metal organic framework material perylene tetracarboxylate magnesium: preparation and biosensing. Nanoscale. 2021;13:16244–50.
77. Shang L, Xu J, Nienhaus GU. Recent advances in synthesizing metal nanocluster-based nanocomposites for application in sensing, imaging and catalysis. Nano Today. 2019;28: 100767.
78. Cao F, Ju E, Liu C, Li W, Zhang Y, Dong K, Liu Z, Ren J, Qu X. Encapsulation of aggregated gold nanoclusters in a metal–organic framework for real-time monitoring of drug release. Nanoscale. 2017;9(12):4128–34.
79. Zhang L, Gao Y, Sun S, Li Z, Wu A, Zeng L. pH-responsive metal–organic framework encapsulated gold nanoclusters with modulated release to enhance photodynamic therapy/chemotherapy in breast cancer. J Mater Chem B. 2020;8(8):1739–47.
80. Ma X, Ren X, Guo X, Fu C, Wu Q, Tan L, Li H, Zhang W, Chen X, Zhong H, Meng X. Multifunctional iron-based metal–organic framework as biodegradable nanozyme for microwave enhancing dynamic therapy. Biomaterials. 2019;214: 119223.
81. Yang D, Yang G, Gai S, He F, An G, Dai Y, Lv R, Yang P. Au-25 cluster functionalized metal–organic nanostructures for magnetically targeted photodynamic/photothermal therapy triggered by single wavelength 808 nm near-infrared light. Nanoscale. 2015;7(46):19568–78.
82. Bian R, Wang T, Zhang L, Li L, Wang C. A combination of tri-modal cancer imaging and in vivo drug delivery by metal–organic framework based composite nanoparticles. Biomater Sci. 2015;3(9):1270–8.
83. Weerapana E, Wang C, Simon GM, Richter F, Khare S, Dillon MBD, Bachovchin DA, Mowen K, Baker D, Cravatt BF. Quantitative reactivity profiling predicts functional cysteines in proteomes. Nature. 2010;468(7325):790–5.
84. Xia M, Sui Y, Guo Y, Zhang Y. Aggregation-induced emission enhancement of gold nanoclusters in metal–organic frameworks for highly sensitive fluorescent detection of bilirubin. Analyst. 2021;146(3):904–10.
85. Jalili R, Dastborhan M, Chenaghlou S, Khataee A. Incorporating of gold nanoclusters into metal–organic frameworks for highly sensitive detection of 3-nitrotyrosine as an oxidative stress biomarker. J Photochem Photobiol A. 2020;391: 112370.
86. Setsukinai KI, Urano Y, Kakinuma K, Majima HJ, Nagano T. Development of novel fluorescence probes that can reliably detect reactive oxygen species and distinguish specific species. J Biol Chem. 2003;278(5):3170–5.
87. Cao X, Cheng S, You Y, Zhang S, Xian Y. Sensitive monitoring and bioimaging intracellular highly reactive oxygen species based on gold nanoclusters@nanoscale metal–organic frameworks. Anal Chim Acta. 2019;1092:108–16.
88. Ugidos-Rodríguez S, Matallana-González MC, Sánchez-Mata MC. Lactose malabsorption and intolerance: a review. Food Funct. 2018;9(8):4056–68.
89. Chen WH, Vázquez-González M, Zoabi A, Abu-Reziq R, Willner I. Biocatalytic cascades driven by enzymes encapsulated in metal–organic framework nanoparticles. Nat Catal. 2018;1(9):689–95.
90. Guo M, Chi J, Zhang C, Wang M, Liang H, Hou J, Ai S, Li X. A simple and sensitive sensor for lactose based on cascade reactions in Au nanoclusters and enzymes co-encapsulated metal–organic frameworks. Food Chem. 2021;339: 127863.
91. Feng L, Yang J, Zhang S, Zhang L, Chen X, Li P, Gao Y, Xie S, Zhang Y, Wang H. A capillary-based fluorimetric platform for the evaluation of glucose in blood using gold nanoclusters and glucose oxidase in the ZIF-8 matrix. Analyst. 2020;145(15):5273–9.
92. Liu FT, Rabinovich GA. Galectins as modulators of tumour progression. Nat Rev Cancer. 2005;5(1):29–41.
93. Zhang X, Zeng Y, Zheng A, Cai Z, Huang A, Zeng J, Liu X, Liu J. A fluorescence based immunoassay for galectin-4 using gold nanoclusters and a composite consisting of glucose oxidase and a metal–organic framework. Microchim Acta. 2017;184(7):1933–40.
94. Tao Y, Lin Y, Ren J, Qu X. A dual fluorometric and colorimetric sensor for dopamine based on BSA-stabilized Aunanoclusters. Biosens Bioelectron. 2013;42:41–6.
95. Dawson TM, Dawson VL. Molecular pathways of neurodegeneration in Parkinson's disease. Science. 2003;302(5646):819–22.
96. Shao K, You J, Ye S, Gu D, Wang T, Teng Y, Shen Z, Pan Z. Gold nanoclusters-poly(9,9-dioctylfluorenyl-2,7-diyl) dots@zeolitic imidazolate framework-8 (ZIF-8) nanohybrid based probe for ratiometric analysis of dopamine. Anal Chim Acta. 2020;1098:102–9.
97. Khataee A, Jalili R, Dastborhan M, Karimi A, Azar AEF. Ratiometric visual detection of tetracycline residues in milk by framework-enhanced fluorescence of gold and copper nanoclusters. Spectrochim Acta A. 2020;242: 118715.
98. Jalili R, Irani-nezhad MH, Khataee A, Joo SW. A ratiometric fluorescent probe based on carbon dots and gold nanocluster encapsulated metal–organic framework for detection of cephalexin residues in milk. Spectrochim Acta A. 2021;262: 120089.
99. Wu YX, Zhang D, Hu X, Peng R, Li J, Zhang X, Tan W. Multicolor two-photon nanosystem for multiplexed intracellular imaging and targeted cancer therapy. Angew Chem Int Ed. 2021;60(22):12569–76.
100. Ma T, Hou Y, Zeng J, Liu C, Zhang P, Jing L, Shangguan D, Gao M. Dual-ratiometric target-triggered fluorescent probe for simultaneous quantitative visualization of tumor microenvironment protease activity and pH in vivo. J Am Chem Soc. 2018;140(1):211–8.
101. Qu A, Sun M, Xu L, Hao C, Wu X, Xu C, Kotov NA, Kuang H. Quantitative zeptomolar imaging of mirna cancer

markers with nanoparticle assemblies. Proc Nat Acad Sci USA. 2019;116(9):3391–400.
102. Peng H, Newbigging AM, Reid MS, Uppal JS, Xu J, Zhang H, Le XC. Signal amplification in living cells: a review of microrna detection and imaging. Anal Chem. 2020;92(1):292–308.
103. Unnikrishnan B, Lien CW, Huang CC. Nanozyme based detection of heavy metal ions and its challenges: a mini review. J Anal Test. 2019;3(3):206–18.
104. Qu W, Yuan W, Li M, Chen Y. A hexaazatriphenylene fused large discotic polycyclic aromatic hydrocarbon with selective and sensitive metal-ion sensing properties. Chin Chem Lett. 2021;32(12):3837–40.
105. Guo M, Chi J, Li Y, Waterhouse GIN, Ai S, Hou J, Li X. Fluorometric determination of mercury(II) based on dual-emission metal–organic frameworks incorporating carbon dots and gold nanoclusters. Microchim Acta. 2020;187(9):534.
106. Li Y, Hu X, Zhang X, Cao H, Huang Y. Unconventional application of gold nanoclusters/Zn-MOF composite for fluorescence turn-on sensitive detection of zinc ion. Anal Chim Acta. 2018;1024:145–52.
107. Wu XJ, Kong F, Zhao CQ, Ding SN. Ratiometric fluorescent nanosensors for ultra-sensitive detection of mercury ions based on AuNCs/MOFs. Analyst. 2019;144(8):2523–30.
108. Tan Q, Zhang R, Zhang G, Liu X, Qu F, Lu L. Embedding carbon dots and gold nanoclusters in metal–organic frameworks for ratiometric fluorescence detection of Cu^{2+}. Anal Bioanal Chem. 2020;412(6):1317–24.
109. Wang K, Qian M, Qi H, Gao Q, Zhang C. Single particle-based confocal laser scanning microscopy for visual detection of copper ions in confined space(dagger). Chin J Chem. 2021;39:1804–10.
110. Lippert AR, New EJ, Chang CJ. Reaction-based fluorescent probes for selective imaging of hydrogen sulfide in living cells. J Am Chem Soc. 2011;133(26):10078–80.
111. Zhao Y, Pan M, Liu F, Liu Y, Dong P, Feng J, Shi T, Liu X. Highly selective and sensitive detection of trinitrotoluene by framework-enhanced fluorescence of gold nanoclusters. Anal Chim Acta. 2020;1106:133–8.
112. Sun F, Liang Y, Jin L, Shi J, Shang L. Weak interaction-tailored catalytic interface of ultrasmall gold nanoclusters as enzyme mimics for enhanced colorimetric biosensing. ACS Appl Mater Interfaces. 2021;13(48):58209–19.
113. Liu L, Song Y, Chong H, Yang S, Xiang J, Jin S, Kang X, Zhang J, Yu H, Zhu M. Size-confined growth of atom-precise nanoclusters in metal–organic frameworks and their catalytic applications. Nanoscale. 2016;8(3):1407–12.
114. Xiao FX, Liu B. In situ etching-induced self-assembly of metal cluster decorated one-dimensional semiconductors for solar-powered water splitting: unraveling cooperative synergy by photoelectrochemical investigations. Nanoscale. 2017;9(43):17118–32.
115. Sun L, Yun Y, Sheng H, Du Y, Ding Y, Wu P, Li P, Zhu M. Rational encapsulation of atomically precise nanoclusters into metal–organic frameworks by electrostatic attraction for CO_2 conversion. J Mater Chem A. 2018;6(31):15371–6.
116. Zhang P, Chen C, Kang X, Zhang L, Wu C, Zhang J, Han B. In situ synthesis of sub-nanometer metal particles on hierarchically porous metal–organic frameworks via interfacial control for highly efficient catalysis. Chem Sci. 2018;9(5):1339–43.
117. Gao G, Xi Q, Zhang Y, Jin M, Zhao Y, Wu C, Zhou H, Guo P, Xu J. Atomic- scale engineering of MOF array confined Au nanoclusters for enhanced heterogeneous catalysis. Nanoscale. 2019;11(3):1169–76.
118. Sim HYF, Chen JRT, Koh CSL, Lee HK, Han X, Phan-Quang GC, Pang JY, Lay CL, Pedireddy S, Phang IY, Yeow EKL, Ling XY. ZIF-induced d-band modification in a bimetallic nanocatalyst: Achieving over 44% efficiency in the ambient nitrogen reduction reaction. Angew Chem Int Ed. 2020;59(39):16997–7003.
119. Yun Y, Sheng H, Bao K, Xu L, Zhang Y, Astruc D, Zhu M. Design and remarkable efficiency of the robust sandwich cluster composite nanocatalysts ZIF-8@Au-25@ZIF-67. J Am Chem Soc. 2020;142(9):4126–30.
120. Zhu Y, Qiu X, Zhao S, Guo J, Zhang X, Zhao W, Shi Y, Tang Z. Structure regulated catalytic performance of gold nanocluster-MOF nanocomposites. Nano Res. 2020;13(7):1928–32.
121. Chi J, Guo M, Zhang C, Zhang Y, Ai S, Hou J, Wu P, Li X. Glucose oxidase and Au nanocluster co-encapsulated metal–organic frameworks as a sensitive colorimetric sensor for glucose based on a cascade reaction. New J Chem. 2020;44(31):13344–9.
122. Hu WC, Younis MR, Zhou Y, Wang C, Xia XH. In situ fabrication of ultrasmall gold nanoparticles/2D MOFs hybrid as nanozyme for antibacterial therapy. Small. 2020;16(23):2000553.
123. Zhao DH, Li CQ, Hou XL, Xie XT, Zhang B, Wu GY, Jin F, Zhao YD, Liu B. Tumor microenvironment-activated theranostics nanozymes for fluorescence imaging and enhanced chemochemodynamic therapy of tumors. ACS Appl Mater Interfaces. 2021;13(47):55780–9.
124. Xu W, Kang Y, Jiao L, Wu Y, Yan H, Li J, Gu W, Song W, Zhu C. Tuning atomically dispersed fe sites in metal–organic frameworks boosts peroxidase-like activity for sensitive biosensing. Nano Micro Lett. 2020;12(1):184.
125. Wu Y, Jiao L, Xu W, Gu W, Zhu C, Du D, Lin Y. Polydopamine-capped bimetallic AuPt hydrogels enable robust biosensor for organophosphorus pesticide detection. Small. 2019;15(17):1900632.
126. Jin R, Kong D, Zhao X, Li H, Yan X, Liu F, Sun P, Du D, Lin Y, Lu G. Tandem catalysis driven by enzymes directed hybrid nanoflowers for on-site ultrasensitive detection of organophosphorus pesticide. Biosens Bioelectron. 2019;141: 111473.
127. Delvaux M, Walcarius A, Demoustier-Champagne S. Bienzyme HRP–GOx-modified gold nanoelectrodes for the sensitive amperometric detection of glucose at low overpotentials. Biosens Bioelectron. 2005;20(8):1587–94.
128. Kwak K, Lee D. Electrochemistry of atomically precise metal nanoclusters. Acc Chem Res. 2019;52(1):12–22.
129. Zhai Q, Li J, Wang E. Recent advances based on nanomaterials as electrochemiluminescence probes for the fabrication of sensors. Chem Electro Chem. 2017;4(7):1639–50.
130. Benavente-García O, Castillo J. Update on uses and properties of citrus flavonoids: New findings in anticancer, cardiovascular, and anti-inflammatory activity. J Agric Food Chem. 2008;56(15):6185–205.
131. Wang B, Anzai JI. Recent progress in electrochemical HbA1c sensors: a review. Materials. 2015;8(3):1187–203.
132. Eissa S, Zourob M. Aptamer- based label-free electrochemical biosensor array for the detection of total and glycated hemoglobin in human whole blood. Sci Rep. 2017;7(1):1016.
133. Dong H, Jin S, Ju H, Hao K, Xu LP, Lu H, Zhang X. Trace and label-free microrna detection using oligonucleotide encapsulated silver nanoclusters as probes. Anal Chem. 2012;84(20):8670–4.
134. Li J, Lin X. Simultaneous determination of dopamine and serotonin on gold nanocluster/overoxidized-polypyrrole composite modified glassy carbon electrode. Sens Actuat B. 2007;124(2):486–93.
135. Harshey A, Srivastava A, Das T, Nigam K, Shrivastava R, Yadav VK. Trends in gunshot residue detection by electrochemical methods for forensic purpose. J Anal Test. 2021;5(3):258–69.
136. Prabhavathi M, Pathakumari B, Raja A. IFN-γ/TNF-α ratio in response to immuno proteomically identified human T-cell antigens of mycobacterium tuberculosis-the most suitable surrogate biomarker for latent tb infection. J Infection. 2015;71(2):238–49.

137. Wang TY, Guo R, Hu LL, Liu JJ, Lu HT. Mass spectrometry-based targeted metabolomics revealed the regulatory roles of magnesium on biofilm formation in escherichia coli by targeting functional metabolites. J Anal Test. 2022. https://doi.org/10.1007/s41664-41021-00208-41666.
138. Bisht A, Mishra A, Bisht H, Tripathi RM. Nanomaterial based biosensors for detection of viruses including sars-cov-2: a review. J Anal Test. 2021;5(4):327–40.
139. Hou Y, Lv CC, Guo YL, Ma XH, Liu W, Jin Y, Li BX, Yang M, Yao SY. Recent advances and applications in paper-based devices for point-of-care testing. J Anal Test. 2022. https://doi.org/10.1007/s41664-41021-00204-w.